Electronic Supplementary Material (ESI) for Journal of Materials Chemistry A.

Supporting Information

Acid induced conversion towards robust and lithiophilic interface for Li-$Li_7La_3Zr_2O_{12}$ solid-state battery

Yadong Ruan,[a,b]†, Yang Lu,[a,b]† Xiao Huang,[a,b] Jianmeng Su,[a,b] Changzhi Sun,[a,b] Jun Jin,[a,b] Zhaoyin Wen [a,b]*

a CAS Key Laboratory of Materials for Energy Conversion, Shanghai Institute of Ceramics, Chinese Academy of Science, Shanghai 200050, P. R. China

b University of Chinese Academy of Science, Beijing 100049, P.R. China

**Corresponding Author. E-mail: zywen@mail.sic.ac.cn*

† These authors contributed equally to this work.

Experimental section

Preparation of LLZTO pellets

Cubic phase $Li_{6.5}La_3Zr_{1.5}Ta_{0.5}O_{12}$ was synthesized by conventional solid-state reaction method as literature.[1] The raw materials $LiOH·H_2O$ (AR), La_2O_3 (99.99%), ZrO_2 (AR), Ta_2O_5 (99.99%) with stoichiometry ratio were mixed by wet ball-milling at 400 rpm for 6 h. Noticeably, 2wt% excess of $LiOH·H_2O$ was added to compensate for the lithium volatilization during the pellet sintering process at high temperature. Before ingredient mixing, La_2O_3 was thoroughly dried by heat treatment at 900°C for 12 h. After dried at 70°C for 10 h, the mixture was calcined at 950°C for 6 h in an alumina crucible. The obtained white powder was the raw LLZTO powder.

Pyrochlore phase $La_2Zr_2O_7$ (LZO) was also synthesized by solid-state reaction method from raw materials of La_2O_3 (99.99%), ZrO_2 (AR) with stoichiometry ratio.[2] The mixed powders were ball milled and calcined at 1500°C for 6 h in an alumina crucible.

4wt% additive LZO powder was mixed with the LLZTO powder via a wet grinding process at 250 rpm for 12 h. After that the slurry was dried at 70°C overnight and sieved over 200 mesh, the powder was uniaxially pressed into pellets using a stainless steel mould (Φ18 mm × 2 mm) and sintered at 1250°C for 0.5 h in a Pt crucible which bottom is covered by parent powder LLZTO. Finally, dense ceramic pellets were obtained and was about ~1.2 mm thick and ~14.0 mm in diameter.

Material characterization

The phase analysis was characterized by powder XRD (Rigaku) using a Cu Kα radiation source operated at 40 kV and 30 mA from 10 to 80 degrees (2theta) with a scan speed of 6 degrees/min

to figure out the phase components during the material preparation. The morphology of the ceramic pellets and Li/LLZTO interface were examined by scanning electron microscope (SEM, Hitachi S-3400) and energy dispersive spectrometer (EDS, INCA Energy, Oxford Instruments, UK). Attenuated total reflectance Fourier transform infrared spectroscopy (ATR-FTIR, NICOLET NEXUS, America) as an important technique to detect the local vibrations of crystal symmetry was applied from a wavenumber of 4000 cm^{-1} to 500 cm^{-1}. X-ray photoelectron spectroscopy (XPS, Thermo scientific ESCALAB 250) was conducted to analyze the chemical composition of anodic interface before and after melting Li and all the spectra were fitted with Gaussian-Lorentzian functions and a Shirley-type background.

Electrochemical characterization

Electrochemical impedance spectroscopy (EIS) measurements were performed on Electrochemical workstation (Autolab PGSTAT302N Netherland) in a frequency range of 1 MHz to 0.1 Hz by applying an AC voltage with an amplitude of 10 mV. All the battery tests were carried out with a battery test system (LAND CT2001A, Wuhan in China). The galvanostatic discharge and charge tests of the batteries were measured using a cutoff voltage window of 2.5 V to 4.0 V, 2.8 V to 4.5 V, 1.5 V to 3.0 V corresponding to LFP, NCM, S/C as the cathode, respectively. All the electrochemical characterizations were operated at 25°C.

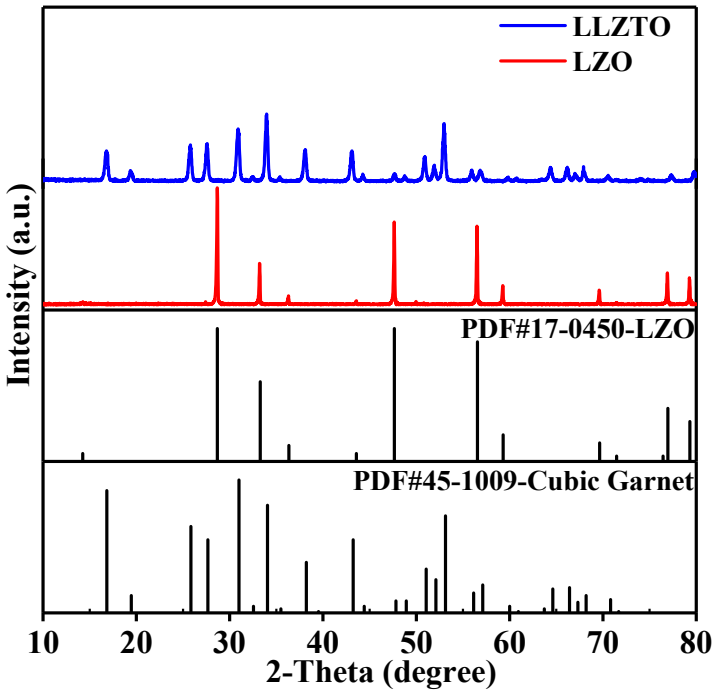

Figure S1. XRD patterns of as-synthesized LLZTO and LZO powder.

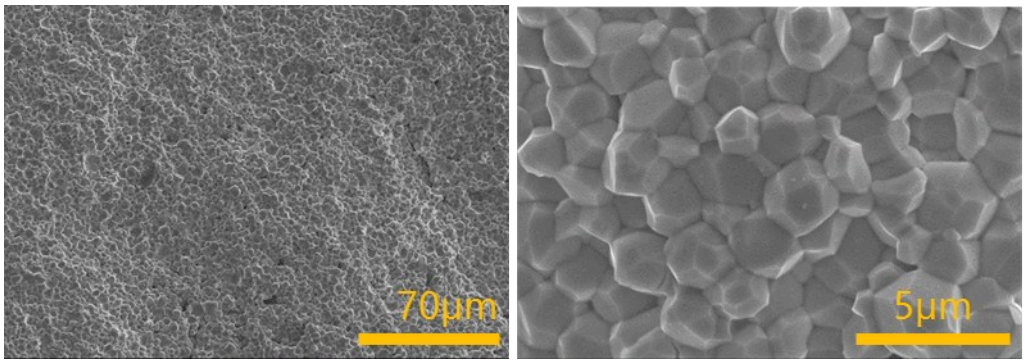

Figure S2. Cross sectional SEM images of a fractured LLZTO pellet at different magnifications.

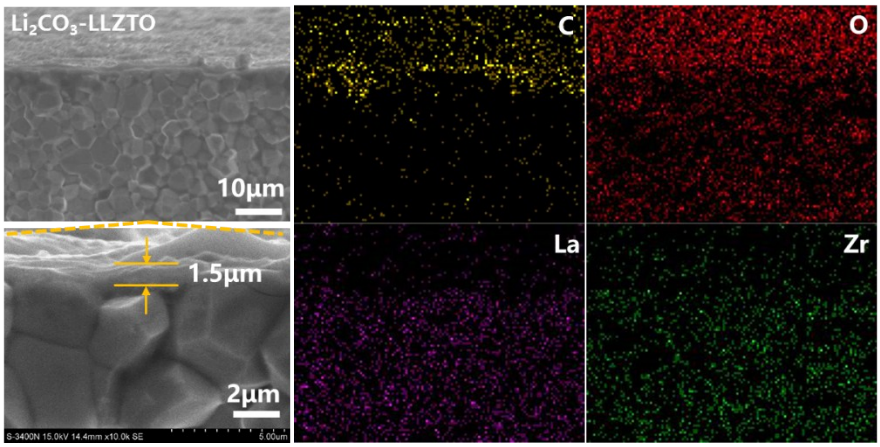

Figure S3. Cross sectional elemental mapping of Li_2CO_3-LLZTO including elemental C, O, La, Zr.

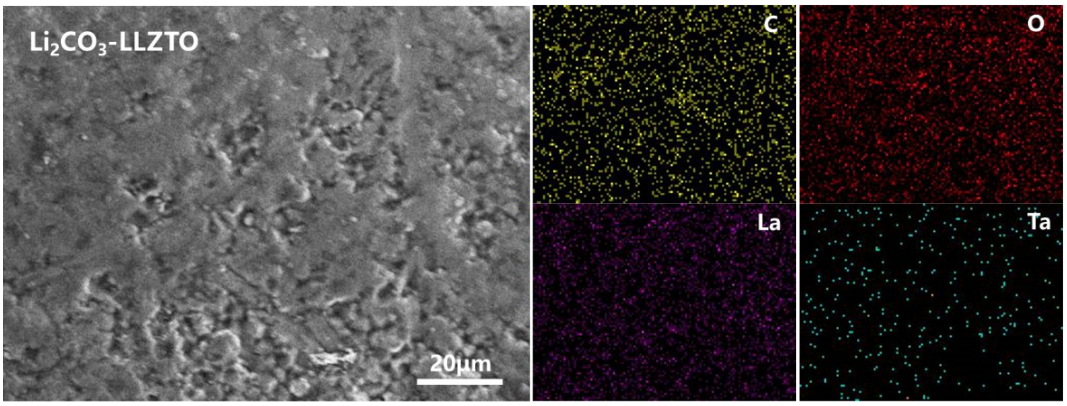

Figure S4. Surface elemental mapping of Li_2CO_3-LLZTO including elemental C, O, La, Ta.

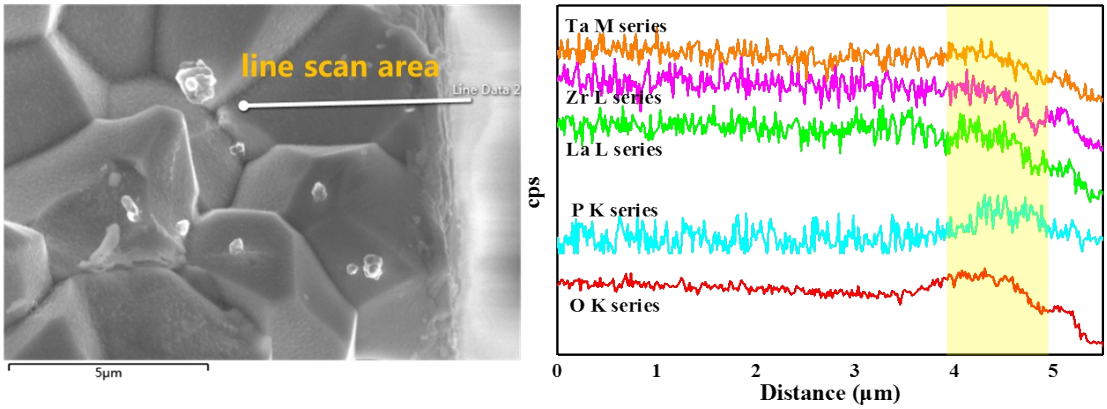

Figure S5. Cross sectional elemental mapping in line scan mode of Li_3PO_4-LLZTO including elemental P, O, La, Zr, Ta.

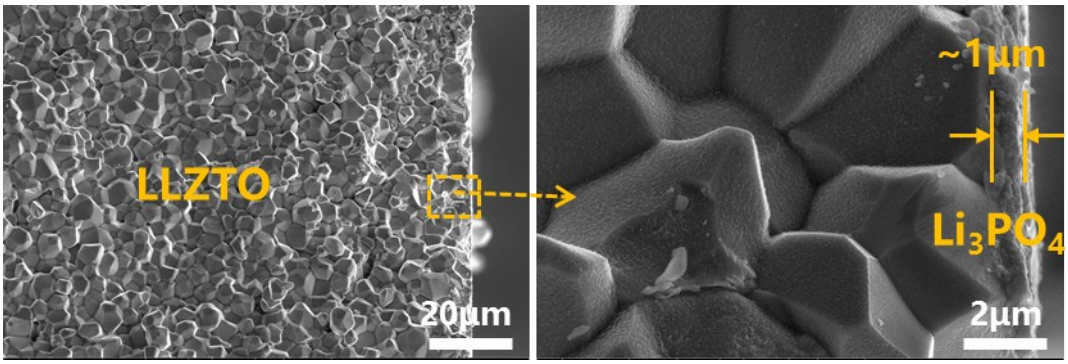

Figure S6. Cross sectional SEM images of Li_3PO_4-LLZTO. It shows clearly that the Li_3PO_4 layer is ~1µm thick.

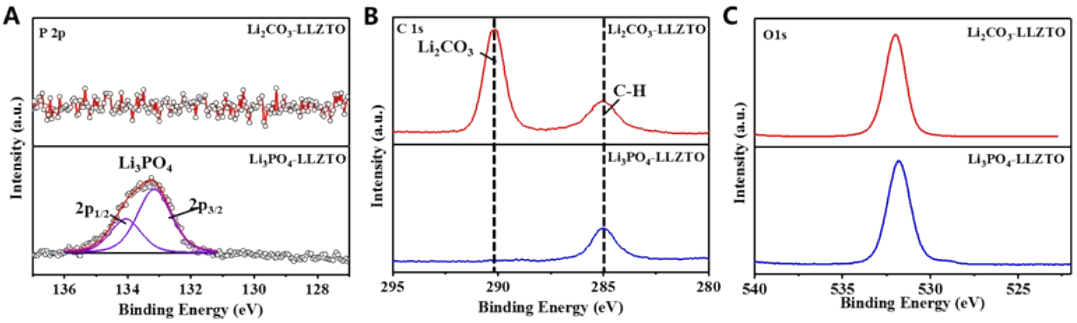

Figure S7. XPS spectra of Li_2CO_3-LLZTO and Li_3PO_4-LLZTO: (A) P 2p; (B) C 1s; (C) O 1s.

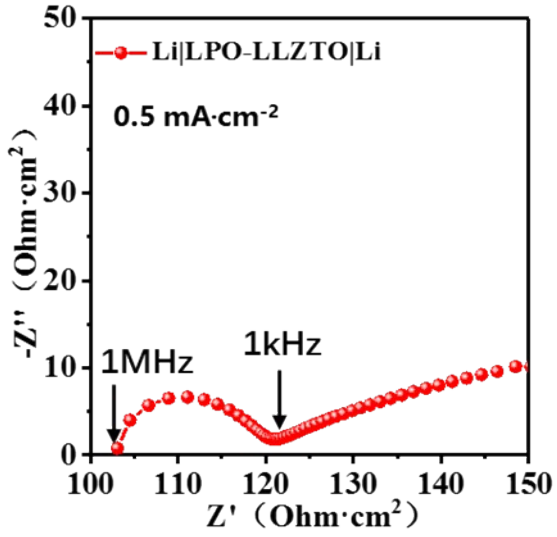

Figure S8. Nyquist plots of Li | Li_3PO_4-LLZTO | Li in the frequency ranging from 1 MHz to 10 mHz at 25°C, which was subsequently measured by galvanostatic cycling at a current density of 0.5 mA cm^{-2}.

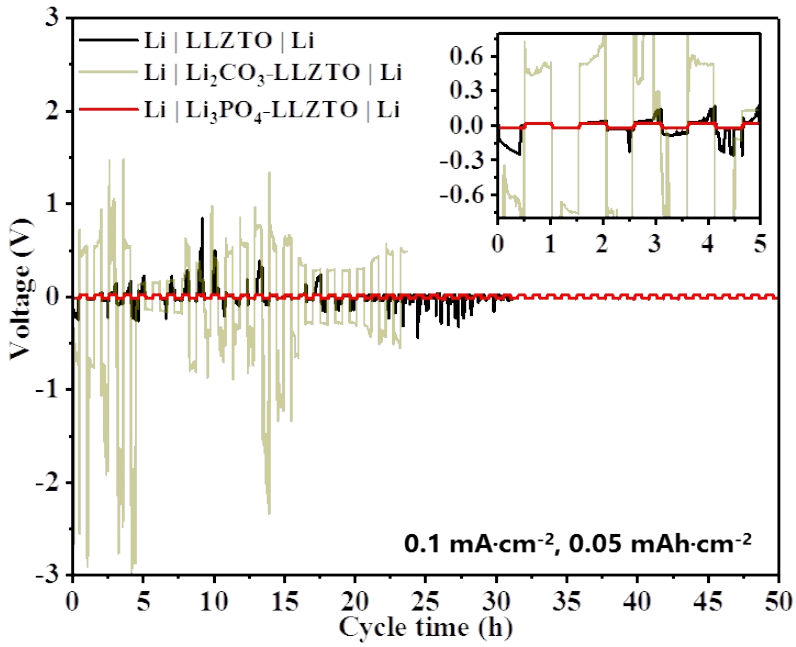

Figure S9. Comparison of galvanostatic cycling of the symmetric cells Li | LLZTO | Li, Li | Li_2CO_3-LLZTO | Li, Li | Li_3PO_4-LLZTO | Li at the current density of 0.1 mA cm^{-2}. The discharge and charge period are half an hour respectively.

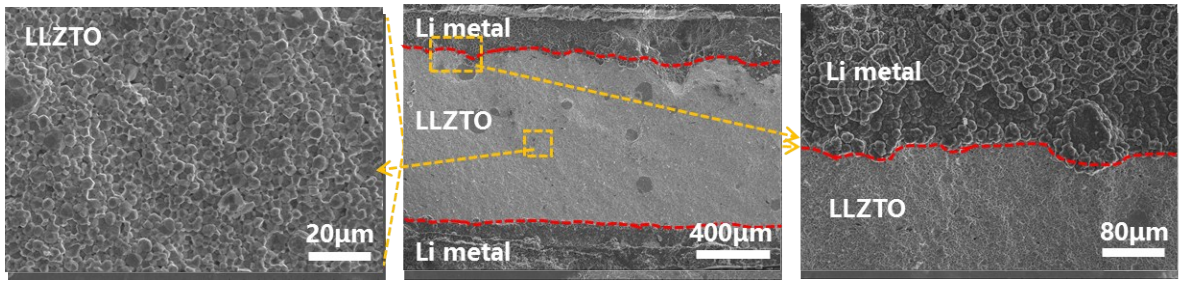

Figure S10. Surface and cross sectional SEM images of Li | Li_3PO_4-LLZTO | Li after long cycles at a current density of 0.5 mA cm^{-2}. The interfacial contacts are still intimate and firm as well as no obvious lithium dendrite penetration is observed inside the LLZTO solid electrolyte.

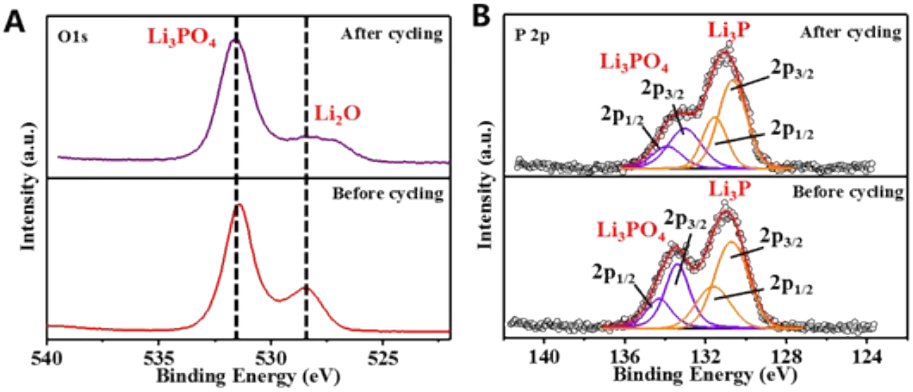

Figure S11. XPS spectra of anodic interface before and after prolonged cycling at a current density of 0.5 mA cm^{-2}: (A) O 1s; (B) P 2p.

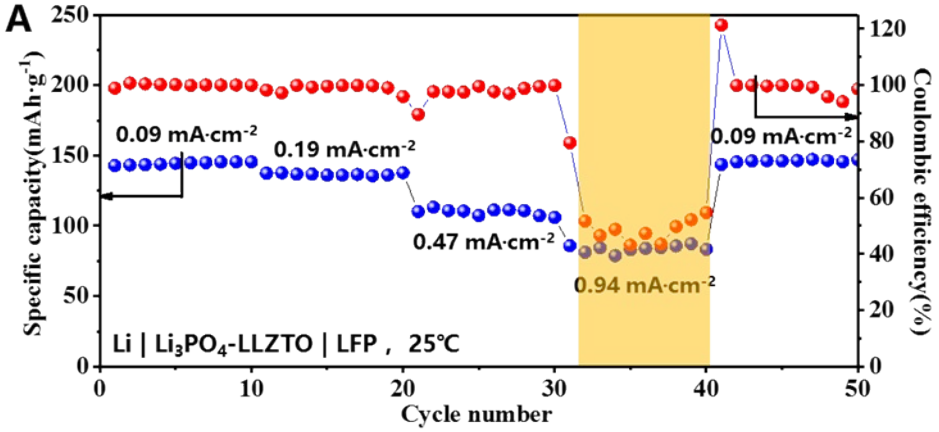

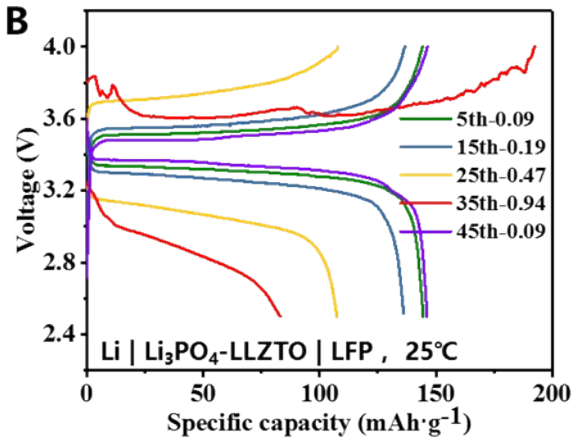

Figure S12. Galvanostatic charge/discharge performance (A) and the corresponding voltage profiles (B) of Li | Li_3PO_4-LLZTO | LFP cell at different current densities.

Table S1. Comparison of advanced anodic modification on garnet based solid state electrolytes (SSEs) by different methods

Solid electrolyte	Modification method	Special apparatus requirement	Li-SSE ASR (Ohm·cm^2)	CCD (mA·cm^{-2})	Cycling performance (mA·cm^{-2}/hours)	Reference
LLZO-0.25Ca, Nb	ALD for Al_2O_3	ALD	34	0.2	0.2/90	[3]
LLZO-0.4Ta	Sputtering Au	Sputter coater	116	0.5 (50ºC)	0.08/150	[4]
LLZO-0.25Ca, Nb	PECVD for Si	PECVD	127	0.2	0.1/225, 0.2/15	[5]
LLZO-0.1Ca-0.25Nb	Evaporating Ge	Evaporator	115	0.1	0.1/100	[6]
LLZO-0.25Ca, Nb	Sputtering Al	Ebeam evaporator	75	0.2	0.1/40, 0.2/41	[7]
LLZO-0.25Ca, Nb	ALD for ZnO	ALD	20	0.1	0.1/50	[8]
LLZO-0.5Ta	Heating treatment	Spark plasma sintering	N/A	0.6	N/A	[9]
LLZO-0.5Ta	Carbon thermal reduction	Heat treatment equipment	45	0.1	0.1/450 (65ºC)	[10]
LLZO-0.2Al, 0.25W	Drawing graphite	No special technique	105	0.3	0.3/1000	[11]
LLZO-0.25Ca, Nb	Sputtering Ag	Magnetron Sputtering	66	0.2	0.1/100, 0.2/100	[12]
LLZO-0.5Ta	Li_3N modification	PECVD	~150	0.15	0.15/50, 0.1/160	[13]
LLZO-0.5Ta-4wt%LZO	H_3PO_4 treatment	No special technique	7	0.8	0.1/1000, 0.5/450	This work

** LLZO-0.25Ca, Nb = $Li_7La_3Zr_2O_{12}$ doped by 0.25 CaO and 0.125 Nb_2O_5 ($Li_7La_{2.75}Ca_{0.25}Zr_{1.75}Nb_{0.25}O_{12}$), CCD (critical current density).*

Table S2. The fitting parameters of XPS spectra on the Li_2CO_3-LLZTO and Li_3PO_4-LLZTO surface.

Peak	Position(eV)	Area	FWHM(eV)	%GL(%)
Li_3PO_4-P $2p_{1/2}$	134.06	1054.955	1.16	39
Li_3PO_4-P $2p_{3/2}$	133.16	2109.91	1.28	32
Li_2CO_3-C 1s	290	N/A	N/A	N/A
C-H-C 1s	285	N/A	N/A	N/A
Li_3PO_4-O 1s	531.85	N/A	N/A	N/A
Li_2CO_3-O 1s	532	N/A	N/A	N/A

Table S3. The fitting parameters of XPS spectra on the Li_3PO_4-LLZTO surface before and after melting Li.

Sample before melting Li	Position(eV)	Area	FWHM(eV)	%GL(%)
Li_3PO_4-P $2p_{1/2}$	134.06	1054.955	1.16	39
Li_3PO_4-P $2p_{3/2}$	133.16	2109.91	1.28	32
Li_3PO_4-O 1s	531.85	N/A	N/A	N/A

Sample after melting Li	Position(eV)	Area	FWHM(eV)	%GL(%)
Li_3PO_4-P $2p_{1/2}$	134.3	572.941	1.488	55
Li_3PO_4-P $2p_{3/2}$	133.4	1145.882	1.45	42
Li_3P-P $2p_{1/2}$	131.615	881.979	2	5
Li_3P-P $2p_{3/2}$	130.715	1763.958	1.98	1
Li_2O-O 1s	528.45	N/A	N/A	N/A
Li_3PO_4-O 1s	531.45	N/A	N/A	N/A

Table S4. Fitting parameters of Li | LLZTO | Li and Li | Li_3PO_4- LLZTO | Li symmetric cell. The fitting circuit and results are presented in Figure 4.

LLZTO	R_b	R_1	CPE_1-Y_0	CPE_1-N	$C_{1pseduo}$
Without Li_3PO_4	143	1126	2.36E-08	0.88511	6.00E-09
With Li_3PO_4	140.52	6.971	1.47E-06	0.90975	4.70E-07

LLZTO	R_2	CPE_2-Y_0	CPE_2-N	$C_{2pseduo}$	χ^2
Without Li_3PO_4	1034.7	7.26E-05	0.39475	1.37E-06	0.017275
With Li_3PO_4	25.047	0.030839	0.2343	1.33E-02	0.0002103

Note: Units in table: R-Ohm·cm², Y_0-Mho, C-F, N, χ^2-None.

Table S5. The fitting parameters of XPS spectra of anodic interface Li/LPO-LLZTO before and after prolonged cycling at the current density of 0.5 mA cm^{-2}.

Sample before cycling	Position(eV)	Area	FWHM(eV)	%GL(%)
Li_3PO_4-O 1s	531.45	N/A	N/A	N/A
Li_2O-O 1s	528.45	N/A	N/A	N/A
Li_3PO_4-P $2p_{1/2}$	134.3	572.941	1.488	55
Li_3PO_4-P $2p_{3/2}$	133.4	1145.882	1.45	42
Li_3P-P $2p_{1/2}$	131.615	881.979	2	5
Li_3P-P $2p_{3/2}$	130.715	1763.958	1.98	1

Sample after cycling	Position(eV)	Area	FWHM(eV)	%GL(%)
Li_3PO_4-O 1s	531.55	N/A	N/A	N/A
Li_3PO_4-P $2p_{1/2}$	134.1	458.595	1.80	25
Li_3PO_4-P $2p_{3/2}$	133.2	917.190	2.00	25
Li_3P-P $2p_{1/2}$	131.6	800.661	1.45	10
Li_3P-P $2p_{3/2}$	130.7	1601.322	1.70	10

References

1. Y. Lu, X. Huang, Z. Song, K. Rui, Q. Wang, S. Gu, J. Yang, T. Xiu, M. E. Badding and Z. Wen, *Energy Storage Materials*, 2018, **15**, 282-290.
2. X. Huang, C. Shen, K. Rui, J. Jin, M. F. Wu, X. W. Wu and Z. Y. Wen, *Jom*, 2016, **68**, 2593-2600.
3. X. Han, Y. Gong, K. K. Fu, X. He, G. T. Hitz, J. Dai, A. Pearse, B. Liu, H. Wang, G. Rubloff, Y. Mo, V. Thangadurai, E. D. Wachsman and L. Hu, *Nat Mater*, 2017, **16**, 572-579.
4. C. L. Tsai, V. Roddatis, C. V. Chandran, Q. Ma, S. Uhlenbruck, M. Bram, P. Heitjans and O. Guillon, *ACS Appl Mater Interfaces*, 2016, **8**, 10617-10626.
5. W. Luo, Y. Gong, Y. Zhu, K. K. Fu, J. Dai, S. D. Lacey, C. Wang, B. Liu, X. Han, Y. Mo, E. D. Wachsman and L. Hu, *J Am Chem Soc*, 2016, **138**, 12258-12262.
6. W. Luo, Y. Gong, Y. Zhu, Y. Li, Y. Yao, Y. Zhang, K. K. Fu, G. Pastel, C. F. Lin, Y. Mo, E. D. Wachsman and L. Hu, *Adv Mater*, 2017, **29**, 1606042.
7. K. K. Fu, Y. Gong, B. Liu, Y. Zhu, S. Xu, Y. Yao, W. Luo, C. Wang, S. D. Lacey, J. Dai, Y. Chen, Y. Mo, E. Wachsman and L. Hu, *Sci Adv*, 2017, **3**, e1601659.
8. C. Wang, Y. Gong, B. Liu, K. Fu, Y. Yao, E. Hitz, Y. Li, J. Dai, S. Xu, W. Luo, E. D. Wachsman and L. Hu, *Nano Lett*, 2017, **17**, 565-571.
9. R. Hongahally Basappa, T. Ito, T. Morimura, R. Bekarevich, K. Mitsuishi and H. Yamada, *Journal of Power Sources*, 2017, **363**, 145-152.
10. Y. Li, X. Chen, A. Dolocan, Z. Cui, S. Xin, L. Xue, H. Xu, K. Park and J. B. Goodenough, *J Am Chem Soc*, 2018, DOI: 10.1021/jacs.8b03106, 6448-6455.
11. Y. J. Shao, H. C. Wang, Z. L. Gong, D. W. Wang, B. Z. Zheng, J. P. Zhu, Y. X. Lu, Y. S. Hu, X. X. Guo, H. Li, X. J. Huang, Y. Yang, C. W. Nan and L. Q. Chen, *Acs Energy Letters*, 2018, **3**, 1212-1218.
12. W. Feng, X. Dong, P. Li, Y. Wang and Y. Xia, *Journal of Power Sources*, 2019, **419**, 91-98.
13. H. Xu, Y. Li, A. Zhou, N. Wu, S. Xin, Z. Li and J. B. Goodenough, *Nano Lett*, 2018, **18**, 7414-7418.